Cellular/Molecular

Ubiquitination of the GluA1 Subunit of AMPA Receptors Is Required for Synaptic Plasticity, Memory, and Cognitive Flexibility

Sumasri Guntupalli,[1,2*] Pojeong Park,[3*] Dae Hee Han,[3*] Lingrui Zhang,[1,2] Xuan Ling Hilary Yong,[1,2] Mitchell Ringuet,[1,2] Daniel G. Blackmore,[1,2] Dhanisha J. Jhaveri,[2,4] Frank Koentgen,[5] Jocelyn Widagdo,[1,2] Bong-Kiun Kaang,[3] and Victor Anggono[1,2]

[1]Clem Jones Centre for Ageing Dementia Research, University of Queensland, Brisbane, Queensland 4072, Australia, [2]Queensland Brain Institute, University of Queensland, Brisbane, Queensland 4072, Australia, [3]School of Biological Sciences, Seoul National University, Seoul, 08826, Korea, [4]Mater Research Institute, University of Queensland, Brisbane, Queensland 4072, Australia, and [5]Ozgene Pty Ltd, Bentley DC, Western Australia 6983, Australia

Activity-dependent changes in the number of AMPA-type glutamate receptors (AMPARs) at the synapse underpin the expression of LTP and LTD, cellular correlates of learning and memory. Post-translational ubiquitination has emerged as a key regulator of the trafficking and surface expression of AMPARs, with ubiquitination of the GluA1 subunit at Lys-868 controlling the post-endocytic sorting of the receptors into the late endosome for degradation, thereby regulating their stability at synapses. However, the physiological significance of GluA1 ubiquitination remains unknown. In this study, we generated mice with a knock-in mutation in the major GluA1 ubiquitination site (K868R) to investigate the role of GluA1 ubiquitination in synaptic plasticity, learning, and memory. Our results reveal that these male mice have normal basal synaptic transmission but exhibit enhanced LTP and deficits in LTD. They also display deficits in short-term spatial memory and cognitive flexibility. These findings underscore the critical roles of GluA1 ubiquitination in bidirectional synaptic plasticity and cognition in male mice.

Key words: **AMPARs; learning and memory; LTD; LTP; synaptic plasticity; ubiquitination**

Significance Statement

Subcellular targeting and membrane trafficking determine the precise number of AMPA-type glutamate receptors at synapses, processes that are essential for synaptic plasticity, learning, and memory. Post-translational ubiquitination of the GluA1 subunit marks AMPARs for degradation, but its functional role *in vivo* remains unknown. Here we demonstrate that the GluA1 ubiquitin-deficient mice exhibit an altered threshold for synaptic plasticity accompanied by deficits in short-term memory and cognitive flexibility. Our findings suggest that activity-dependent ubiquitination of GluA1 fine-tunes the optimal number of synaptic AMPARs required for bidirectional synaptic plasticity and cognition in male mice. Given that increases in amyloid-β cause excessive ubiquitination of GluA1, inhibiting that GluA1 ubiquitination may have the potential to ameliorate amyloid-β-induced synaptic depression in Alzheimer's disease.

Received Aug. 12, 2022; revised June 14, 2023; accepted June 28, 2023.

Author contributions: S.G., P.P., D.H.H., L.Z., X.L.H.Y., and M.R. performed research; S.G., P.P., D.H.H., L.Z., X.L.H.Y., J.W., B.-K.K., and V.A. analyzed data; S.G., P.P., D.H.H., D.G.B., D.J.J., J.W., and B.-K.K. edited the paper; D.G.B., D.J.J., J.W., B.-K.K., and V.A. designed research; F.K. contributed unpublished reagents/analytic tools; V.A. wrote the paper.

This work was supported by Australian Medical Research Future Fund Clem Jones Centre for Ageing Dementia Research Flagship Project Grant; John T. Reid Charitable Trusts to V.A.; and National Honor Scientist Program NRF-2012R1A3A1050385 of Korea to B.-K.K. V.A. holds an Australian Research Council Future Fellowship FT220100485. J.W. was supported by a University of Queensland Amplify award and Australian Research Council Discovery Early Career Researcher Award DE170100112. S.G. was a recipient of a University of Queensland International Scholarship. L.Z. was supported by a University of Queensland Research Training Scholarship. X.L.H.Y. was supported by a Research Training Program Scholarship from the Australian Government and University of Queensland, as well as the Ian Lindenmayer PhD Top-up Scholarship. Imaging was performed at the Queensland Brain Institute's Advanced Microscopy Facility. We thank Dr. Richard Huganir (Johns Hopkins University, Baltimore) for providing antibodies; and Rowan Tweedale for editing this manuscript.

*S.G., P.P., and D.H.H. contributed equally to this work as first authors.

The authors declare no competing financial interests.

Correspondence should be addressed to Victor Anggono at v.anggono@uq.edu.au or Bong-Kiun Kaang at kaang@snu.ac.kr.

https://doi.org/10.1523/JNEUROSCI.1542-22.2023

Introduction

Long-lasting changes in synaptic transmission, termed synaptic plasticity, have long been considered a cellular model of learning and memory (Huganir and Nicoll, 2013). LTP and LTD are two forms of synaptic plasticity that have been intensively studied in this context. Key molecular events underlying the expression of LTP and LTD involve an increase or decrease in the number of AMPARs at the postsynaptic membrane, respectively (Anggono and Huganir, 2012). GluA1 is one of the predominant subunits expressed in the hippocampus and cortex (Lu et al., 2009). GluA1 KO mice display profound deficits in hippocampal LTP, and working and spatial memory (Zamanillo et al., 1999; Sanderson et al., 2007, 2010), underscoring the importance of GluA1-containing AMPARs in synaptic plasticity and cognition.

The C-terminal domain of GluA1 contains multiple sites for protein–protein interaction and post-translational modifications that are critical in regulating the membrane trafficking of AMPARs (Anggono and Huganir, 2012; Lu and Roche, 2012; Diering and Huganir, 2018). Reversible post-translational modifications, such as phosphorylation, palmitoylation, and ubiquitination in the GluA1 subunit provide fine-tuning mechanisms that control synaptic expression of the receptors (Lussier et al., 2015; Widagdo et al., 2017; Diering and Huganir, 2018; Hayashi, 2021). The best characterized among these is the phosphorylation of GluA1 at the Ser-831 and Ser-845 residues, which are known to control AMPAR trafficking and gating in neurons (Hu et al., 2007; Man et al., 2007; Kristensen et al., 2011). These phosphorylation sites are tightly regulated during LTP and LTD (Lee et al., 2000). Pseudophosphorylation of GluA1 at Ser-831 and Ser-845 is sufficient to lower the threshold for LTP induction in the GluA1 S831/S845D phosphomimetic knock-in mouse (Makino et al., 2011). Furthermore, GluA1 S831/845A phospho-deficient knock-in mice show deficits in LTP and LTD, as well as memory defects in spatial learning tasks (Lee et al., 2003). This evidence highlights the importance of GluA1 phosphorylation events at these residues for synaptic plasticity, learning, and memory.

Post-translational ubiquitination has emerged as an important mechanism that regulates the surface expression of AMPARs (Goo et al., 2015; Widagdo et al., 2015; Mabb, 2021). There is also considerable functional cross-talk between the ubiquitination and phosphorylation of different AMPAR subunits (Guntupalli et al., 2017; Widagdo et al., 2020). Activity-dependent ubiquitination of GluA1 has been shown to occur at the C-terminal Lys-868 residue and is primarily mediated by E3 ligases, Nedd4-1, Nedd4-2, and RNF220 (Schwarz et al., 2010; Lin et al., 2011; Zhu et al., 2017; Ma et al., 2022). GluA1 ubiquitination controls the post-endocytic sorting of AMPARs toward late endosomes for degradation (Schwarz et al., 2010; Lin et al., 2011; Widagdo et al., 2015, 2017). In pathologic conditions, excessive ubiquitination of GluA1 mediates amyloid-β (Aβ)-induced downregulation of surface AMPAR expression, leading to synaptic depression (Rodrigues et al., 2016; Guntupalli et al., 2017; Zhang et al., 2018). However, the physiological functions of GluA1 ubiquitination in synaptic plasticity, learning, and memory remain unknown. Here, we report the generation and characterization of a knock-in mouse harboring the K868R mutation in the *Gria1* gene that encodes the GluA1 subunit of AMPARs.

Materials and Methods

Antibodies. Antibodies were purchased from commercial sources as follows: anti-β-actin (clone 13E5, Cell Signaling Technology), anti-GluA1 (clone RH95, Merck), anti-PSD-95 (clone K28/43, NeuroMab), anti-synaptophysin (#101011, Synaptic Systems), and anti-ubiquitin (clone P4D1, Santa Cruz Biotechnology). Antibodies against GluA1 (clone 4.9D) and GluA2 (clone 6A) were gifts from Dr. Richard Huganir (Widagdo et al., 2015).

Animals. All experimental procedures conducted on animals in this study were approved by the University of Queensland Animal Ethics Committee (QBI/047/18) and the Seoul National University Institutional Animal Care and Use Committee (SNU-130526-1-7). The GluA1 K868R knock-in mouse was generated using the conventional homologous recombination method in C57Bl/6 embryonic stem cells. The targeting vector comprised an artificial WT exon 16, flanked by inverted LoxP2272 and FRT sites, followed by a neomycin cassette, an FRT site, an inversed exon 16 containing the Lys-868 substitution to arginine (K868R), and an inverted LoxP2272 flanked by a pair of inverted LoxP sites (see Fig. 1*A*). This construct was electroporated into embryonic stem cells. Positive clones were identified by PCR and Southern blotting using the 5′, 3′ and neomycin probes. Positive clones were injected into C57Bl/6 blastocysts, and chimeras were crossed to OzFlp mice to remove the neo cassette from the germline. After confirmation of *neo* excision by Southern blot analysis, heterozygous conditional knock-in mice were backcrossed to C57Bl/6 animals to remove the *Flp* gene and the resulting conditional knock-in mice were bred to homozygosity. The *Flp*-negative mice were subsequently bred to CMV-Cre mice (Schwenk et al., 1995) to obtain the GluA1 K868R knock-in heterozygous offspring. The *Cre* gene was then bred out by crossing these offspring to C57Bl/6 mice. The *Flp*- and *Cre*-negative GluA1 K868R knock-in mice were maintained as heterozygous mating.

Genotyping. Genotyping of GluA1 knock-in mice was conducted by PCR of genomic DNA isolated from ear or toe biopsies using three primers: primer 1 (5′-ATGGCAGAGTGGTCAGCCAG-3′), primer 2 (5′-TTTGGCACTGAAGGGCTTGG-3′), and primer 3 (5′-GCTATCCGG ACCAGTACACT-3′). The WT allele produces a band of 172 bp, whereas the knock-in allele yields a 222 bp product when resolved on a 3% agarose gel. PCR fragments were sent for sequencing to validate the presence of a knock-in mutation.

Primary cortical neuronal cultures. Cortices derived from embryonic day 17 mouse pups of unknown sex, either from WT or GluA1 K868R knock-in mice, were used to generate primary neuronal cultures (Widagdo et al., 2015). Cortices were isolated and dissociated with 30 U of papain suspension (Worthington) for 20 min in a 37°C water bath. A single-cell suspension was obtained by triturating tissues with fire-polished glass Pasteur pipettes and then plated at a density of 1.2×10^6 cells on poly-L-lysine-coated 6 cm tissue culture dishes in a Neurobasal growth medium (Invitrogen) supplemented with 2 mM Glutamax, 1% penicillin/streptomycin, 2% B27, and 5% FCS. Cortical neurons were maintained in a Neurobasal medium containing 1% FBS and fed twice a week. Uridine (Sigma, 5 μM) and 5′-fluoro-2′-deoxyuridine (Sigma, 5 μM) were added to the culture medium at DIV 5 to stop glial proliferation. Cells were processed at DIV 14-16.

Subcellular fractionation. Forebrains were isolated from mice and homogenized in ice-cold sucrose buffer A (0.32 M sucrose, 10 mM HEPES, pH 7.4). The homogenate was centrifuged at 1000 × *g* for 10 min at 4°C, yielding the supernatant fraction and the nuclear-enriched pellet. An aliquot of the homogenate was taken for further analysis as the total protein fraction, with the remainder being centrifuged at 10,000 × *g* for 15 min at 4°C to obtain a crude synaptosomal (P2) fraction and cytosolic protein-enriched supernatant (S2). The P2 fraction was resuspended with sucrose buffer and centrifuged at 10,000 × *g* for 15 min at 4°C. The resulting pellets were lysed by hypo-osmotic shock in ice-cold water and homogenized by pipetting; 1 M HEPES was rapidly added to a final concentration of 4 mM to adjust the pH. The P2 suspension was incubated by rotating in the cold room for 30 min before an ultracentrifugation step at 25,000 × *g* for 20 min. The resulting pellet (LP1) was further resuspended in buffer B (50 mM HEPES, 2 mM EDTA, pH 7.4) containing 1% Triton X-100 and mixed in a cold room for 15 min. This LP1

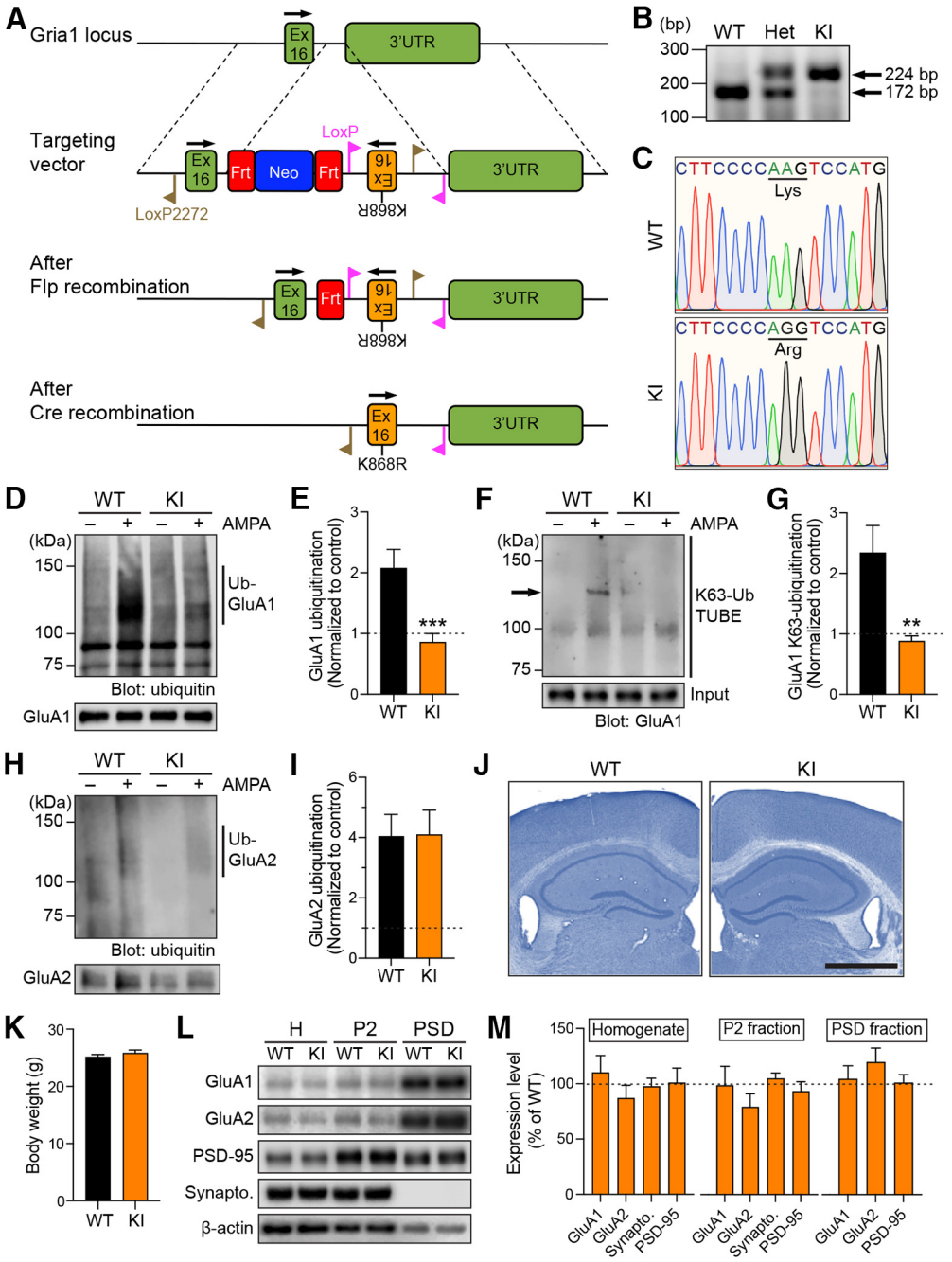

Figure 1. Normal gross anatomy and distribution of GluA1 and GluA2 subunits in the forebrain of GluA1 K868R knock-in mice. ***A***, Schematic representation of the genomic DNA structure of the *Gria1* locus that encodes the C-terminal tail of the GluA1 protein, the targeting vector, and the resulting genomic structures following Flp- and Cre-mediated recombination events. Ex, Exon; UTR, untranslated region; Frt, flippase target site; Neo, neomycin gene. ***B***, PCR analysis of genomic DNA samples from WT, heterozygous (Het), and homozygous knock-in (KI) mutant mice. ***C***, Verification of the GluA1 K868R mutation in homozygous KI mice, and its absence in WT mice by DNA sequencing. ***D***, Primary cortical neurons derived from WT or GluA1 K868R KI mice were incubated in the presence or absence of 100 μM AMPA, lysed, and immunoprecipitated with anti-GluA1 antibodies. Eluted proteins were subjected to Western blot analysis and probed with anti-ubiquitin and anti-GluA1 antibodies. ***E***, Quantification of the levels of AMPA-induced GluA1 ubiquitination normalized to the controls (dashed line). Data are mean ± SEM (WT, $n = 9$; KI, $n = 8$ per group). ***$p = 0.0006$ (Mann–Whitney test). ***F***, Primary cortical neurons derived from WT or GluA1 K868R KI mice were incubated in the presence or absence of 100 μM AMPA, lysed, and incubated with biotinylated K63-linked TUBE (Tandem Ubiquitin Binding Entities) precoupled to Neutravidin agarose beads. Eluted proteins were subjected to Western blot analysis and probed with anti-GluA1 antibodies. Arrow indicates the GluA1 band. ***G***, Quantification of the levels of AMPA-induced GluA1 K63-linked ubiquitination normalized to the controls (dashed line). Data are mean ± SEM (WT, $n = 6$; KI, $n = 4$ per group). **$p = 0.0095$ (Mann–Whitney test). ***H***, Primary cortical neurons derived from WT or GluA1 K868R KI mice were incubated in the presence or absence of 100 μM AMPA, lysed, and immunoprecipitated with anti-GluA2 antibodies. Eluted proteins were subjected to Western blot analysis and probed with anti-ubiquitin and anti-GluA2 antibodies. ***I***, Quantification of the levels of AMPA-induced GluA2 ubiquitination normalized to the controls (dashed line). Data are mean ± SEM ($n = 6$ per group). $p > 0.99$ (Mann–Whitney test). ***J***, Nissl-stained hippocampal sections of GluA1 WT and KI mouse brains show normal cytoarchitecture. Scale bar, 1 mm. ***K***, No differences were observed in the body weights of GluA1 WT and KI mice. Data are mean ± SEM ($n = 15$ per group). $p = 0.49$ (Mann–Whitney test). ***L***, Whole forebrain lysates (H, total homogenate), crude synaptosomes (P2), and PSD fractions from 3-month-old GluA1 KI and WT mice were immunoblotted with specific antibodies against GluA1, GluA2, synaptophysin, PSD-95, and β-actin. ***M***, Quantification of the levels of GluA1, GluA2, synaptophysin, and PSD-95 in each fraction after normalization with β-actin. The average protein expression levels in the GluA1 KI mice were normalized to those of WT mice (dashed line). Data are mean ± SEM ($n = 7$-13 per group).

suspension was then centrifuged at 32,000 × *g* for 20 min to obtain the postsynaptic density (PSD) pellet. All fractions were denatured after adjusting total protein concentrations, followed by Western blotting.

Ubiquitination assay. Ubiquitination of GluA1 and GluA2 was induced by incubating neurons in ACSF containing 100 μM AMPA (Tocris) plus 50 μM D-APV (Hello Bio) and 1 μM TTX (Abcam) for 10 min at 37°C (Widagdo et al., 2015). Neurons were lysed in warm 1% SDS (in PBS) and diluted in 10 volumes of ice-cold cell lysis buffer (1% Triton X-100, 1 mM EDTA, 1 mM EGTA, 50 mM NaF, and 5 mM Na-pyro-phosphate in PBS) supplemented with 10 mM *N*-ethylmaleimide, 20 μM 10 PR-619 (Sigma), 1 mM 1,10-phenanthroline (Sigma), and Complete EDTA-free protease inhibitor cocktails (Sigma). Lysates were centrifuged at 14,000 rpm for 20 min at 4°C and cleared with protein G-Sepharose beads (GE Healthcare). Precleared lysates were then incubated with GluA1 or GluA2 antibodies coupled to protein G-Sepharose overnight at 4°C, followed by four washes with ice-cold lysis buffer and elution in 2× SDS sample buffer. The immunoprecipitated proteins were resolved by SDS-PAGE and probed by Western blot analysis with specific antibodies against GluA1, GluA2, and ubiquitin. The levels of activity-induced ubiquitination were quantified by measuring the ratio of the mean intensities of the ubiquitin bands, divided by the mean intensities of the corresponding immunoprecipitated GluA1 or GluA2 bands from the AMPA- and vehicle-treated groups in neurons derived from WT or GluA1 K868R knock-in mice.

To determine the level of K63-linked ubiquitination of GluA1, neuronal lysates were precleared with Neutravidin agarose beads (Fisher Scientific). Precleared lysates were then incubated with biotinylated K63-TUBE (Tandem Ubiquitin Binding Entities, Life Sensors) precoupled to Neutravidin agarose beads (Fisher Scientific) overnight at 4°C. Beads were washed with ice-cold lysis buffer and eluted in 2× SDS sample buffer. Bound proteins were resolved by SDS-PAGE and probed by Western blot analysis with specific antibodies against GluA1.

Western blot. Protein samples were resolved on 6%, 10%, or 15% SDS polyacrylamide gels and transferred to a PVDF membrane (Millipore) at 100 V for 2 h. Membranes were blocked with 5% skim milk in Tris-buffered saline containing 0.01% Tween-20 for 1 h and incubated with primary antibody overnight at 4°C. After extensive washing with 1% skim milk, HRP-conjugated secondary antibodies were added and incubated for 1 h at room temperature under constant shaking. Signals were developed with an enhanced chemiluminescence method. Images were acquired on the Odyssey Fc imaging system (LI-COR) and band intensities were quantified using Image Studio Lite software (LI-COR).

Nissl staining. Mice were deeply anesthetized and transcardially perfused with PBS, followed by a 4% PFA solution. Dissected brains were immersed in 4% PFA for 24 h. They were then washed 3 times with distilled water, immersed in PBS containing sodium azide as a preservative, and stored at 4°C until used. Brains were sliced coronally using a vibratome at a thickness of 50 μm. Sections were mounted on glass slides and stained with 0.1% cresyl violet for 5 min. Images were taken using a scanning bright-field microscope.

Electrophysiological recordings. Adult male mice were used for all electrophysiological recordings (2-5 months of age). Animals were deeply anesthetized with isoflurane and killed by decapitation. Transverse hippocampal slices (350 μm) were prepared using a vibratome (Leica, VT1200S) in an ice-chilled slicing solution that contained the following (in mM): 210 sucrose, 3 KCl, 26 $NaHCO_3$, 1.25 NaH_2PO_4, 5 $MgSO_4$, 10 D-glucose, 3 sodium ascorbate, and 0.5 $CaCl_2$, saturated with 95% O_2 and 5% CO_2. The slices were transferred to an incubation chamber that contained the recording solution (ACSF) as follows (in mM): 124 NaCl, 3 KCl, 26 $NaHCO_3$, 1.25 NaH_2PO_4, 2 $MgSO_4$, 10 D-glucose, and 2 $CaCl_2$ (carbonated with 95% O_2 and 5% CO_2). Slices were allowed to recover at 32°C-34°C for 30 min and then maintained at 26°C-28°C for a minimum of 1 h before recordings were made.

Standard extracellular recordings were performed in the CA1 region of the hippocampal slices maintained at 32°C, as described previously (Park et al., 2016), to measure the slope of the evoked fEPSPs. Responses were obtained using a Multiclamp 700B amplifier (Molecular Devices) and digitized with a Digidata 1322A A/D board at a sampling rate of 20 kHz (low-pass filtered at 10 kHz). Recordings were monitored and analyzed using WinLTP (Anderson and Collingridge, 2007). Schaffer collateral-commissural pathways were stimulated at a baseline frequency of 0.1 Hz. After a stable baseline of at least 20 min, LTP was induced using theta-burst stimulation (TBS) delivered at the basal stimulus intensity. An episode of TBS comprised five bursts at 5 Hz, with each burst composed of 5 pulses at 100 Hz. Either a single episode of TBS or a train of three TBS episodes at an interepisode interval of 10 min was given. LTD was induced using a repetitive low-frequency stimulation (LFS) at 1 Hz for 15 min, where postnatal day 14 (P14) mice were used for a reliable LFS-LTD induction. DHPG-LTD was induced by the bath application of DHPG (100 μM, Hello Bio) in the presence of D-APV (50 μM) to prevent nonspecific NMDAR-mediated effects. Representative sample traces were an average of four consecutive responses, collected from typical experiments (stimulus artifacts were blanked for clarity). The input–output relationships were estimated by varying the stimulus intensity from 1.5 to 15 V in 1.5 V increments. Paired-pulse facilitation was ranged at interstimulus intervals from 20 to 400 ms at the basal stimulus intensity.

Whole-cell recording was performed at 32°C during continuous perfusion at 3-4 ml/min with ACSF that contained 50 μM picrotoxin (Hello Bio) and 10 μM (+)-bicuculline (Hello Bio) to prevent $GABA_A$ receptor-mediated transmission. CA1 pyramidal cells were visualized with IR-DIC optics (Olympus). The whole-cell solution comprised the following (mM): 8 NaCl, 130 $CsMeSO_3$, 10 HEPES, 0.5 EGTA, 4 Mg-ATP, 0.3 Na_3-GTP, 5 QX-314, and 0.1 spermine. The pH was adjusted to 7.2-7.3 with CsOH, and osmolarity was set to 285-290 mOsm/l. The Schaffer collateral-commissural pathway was stimulated at a constant frequency of 0.1 Hz. Borosilicate glass pipettes were used with a resistance of 4-6 MΩ, and experiments were only accepted for analysis if series resistance values were <25 MΩ and varied by <20% during the course of the experiment. Signals were filtered at 10 kHz and digitized at 20 kHz using a Multiclamp 700B (Molecular Devices). Evoked EPSCs were monitored and analyzed using WinLTP. For NMDA/AMPA ratio, cells were clamped at a holding potential of −70 mV to measure the peak of AMPAR-mediated synaptic transmission. NMDAR-mediated currents were estimated at 50 ms after the stimulation onset at 40 mV of holding potential. Averages of 15 consecutive responses obtained at these holding potentials were used for the ratio. For rectification index measurements, AMPAR-mediated currents were pharmacologically isolated using a combination of a competitive NMDAR antagonist (D-APV; 50 μM) plus a glycine-site antagonist (L-689560; 5 μM, Tocris). Neurons were immediately depolarized to 40 mV for 100 s, then to 0 mV for 50 s, and consecutive responses obtained at these holding potentials were averaged and calculated by taking the ratio of the slopes from 0 to 40 mV and −70 to 0 mV. The amplitude and frequency of miniature EPSCs were analyzed using Mini Analysis (Synaptosoft) from the data obtained for 3 min at a holding potential of −70 mV in the presence of TTX (0.5 μM).

Animal handling. Mice were maintained under standard conditions on a 12 h light/dark cycle (lights on at 7:00 A.M.) with food and water provided *ad libitum*. All behavioral experiments were conducted between 9:00 A.M. and 5:00 P.M. The mice were group-housed with 2-5 animals per cage. Approximately 12- to 15-week-old littermate pairs of WT and knock-in male mice were used for all experiments. Mice were handled for 3 min per day for 3 consecutive days before the commencement of experiments.

Elevated plus maze. An elevated plus maze was used to determine anxiety-related behavior. The apparatus was a plus-shaped opaque Perspex elevated platform with two open (64.5 × 6.2 cm) and two enclosed arms (64.5 × 6.2 cm) radiating from the center platform. The apparatus was placed under an overhead camera to track the animal's movement. Lighting conditions (400 lux) were kept constant throughout the experiment. Mice were placed in the middle of the maze and allowed to explore for 5 min. Recorded videos were analyzed using Ethovision XT9 image analysis software. The number of entries and time spent in the closed and open arms were determined for each animal.

Open field test. The open field test was used to assay locomotor activity and anxiety-like behavior. This test was conducted in a square arena (30.7 × 30.7 × 30.7 cm) placed underneath an overhead camera that tracked the animal's movement. Lighting conditions (400 lux) were kept constant throughout the experiment. In an individual experiment, each mouse was placed in the center of the arena and allowed to explore for 3 min. Recorded videos were analyzed using Ethovision XT9 image analysis software. The total distance traveled was measured for the duration of the trial, together with the time spent in and the number of entries into the center of the arena.

Y maze. A Y maze with a blocked arm was used to measure short-term spatial memory in mice. The apparatus comprised three arms made of Perspex elevated above the floor and was placed under an overhead camera. Lighting conditions (400 lux) were kept constant throughout the experiment. In the first trial, mice were placed in the starting arm and allowed to explore the open arm for 5 min. The second trial began 90 min later in which mice were placed back into the starting arm of the maze with the Perspex divider removed. Mice were allowed to explore all arms for 5 min. Recorded videos were analyzed using Ethovision XT9 image analysis software (Noldus). The number of entries and time spent in the starting and novel arms were determined for each animal.

Active place avoidance test. The active place avoidance task is a hippocampal-dependent spatial learning test for rodents (Willis et al., 2017). This task was performed on an elevated rotating circular arena (at 1 rotation per min) located in a room with visual cues on the walls. The arena contained a 60° shock zone with an electric grid that delivered a brief foot shock (0.5 mA for 500 ms) on animal entry. A second foot shock was delivered at 1.5 s intervals if the animal remained in the shock zone. The position of the shock zone was kept constant relative to the spatial frame of the room. One day after habituation, mice were tested for 10 min in each training session over 5 d. The position of the animal was tracked using an overhead camera linked to Tracker software (Bio-Signal group). To assess the cognitive flexibility of mice, we also performed a reversal test on day 6, in which the position of the shock zone was moved opposite to the initial location. Mice were tested for 10 min in each session for a further 5 d. The number of entries into the shock zone and the distance traveled were measured to determine the extent of learning.

Statistical analysis. All statistical analyses were performed using Prism8 software (GraphPad Software). Comparison between individual experimental groups was performed by unpaired Student's t test or Mann–Whitney test where appropriate. Comparison of more than two parameters/multiple groups was performed by two-way ANOVA with Sidak's multiple comparison test. All graphs were presented as mean ± SEM. The difference between means from experimental groups was considered significant at the level of $p < 0.05$.

Results

GluA1 K868R ubiquitin-deficient mice have normal gross brain morphology and AMPAR distribution at synapses

To directly test whether GluA1 ubiquitination is necessary for synaptic plasticity, learning, and memory, we generated a mutant mouse line that contains an arginine substitution at the major GluA1 ubiquitination site, Lys-868, by targeting the mouse *Gria1* gene using the homologous recombination technique (Fig. 1*A*). Chimera mice carrying the mutant allele were bred to CMV-Cre mice to generate the conventional GluA1 K868R knock-in mice. The success of these procedures was confirmed by PCR analysis and direct DNA sequencing (Fig. 1*B*,*C*). We further confirmed the effect of the mutation on ligand-induced GluA1 ubiquitination in primary cortical neurons derived from WT or GluA1 K868R knock-in mice. As expected, a 10 min treatment of AMPA induced an increase in the levels of GluA1 ubiquitination in the WT neurons, but not in those derived from GluA1 knock-in mice (Fig. 1*D*,*E*). We also revealed

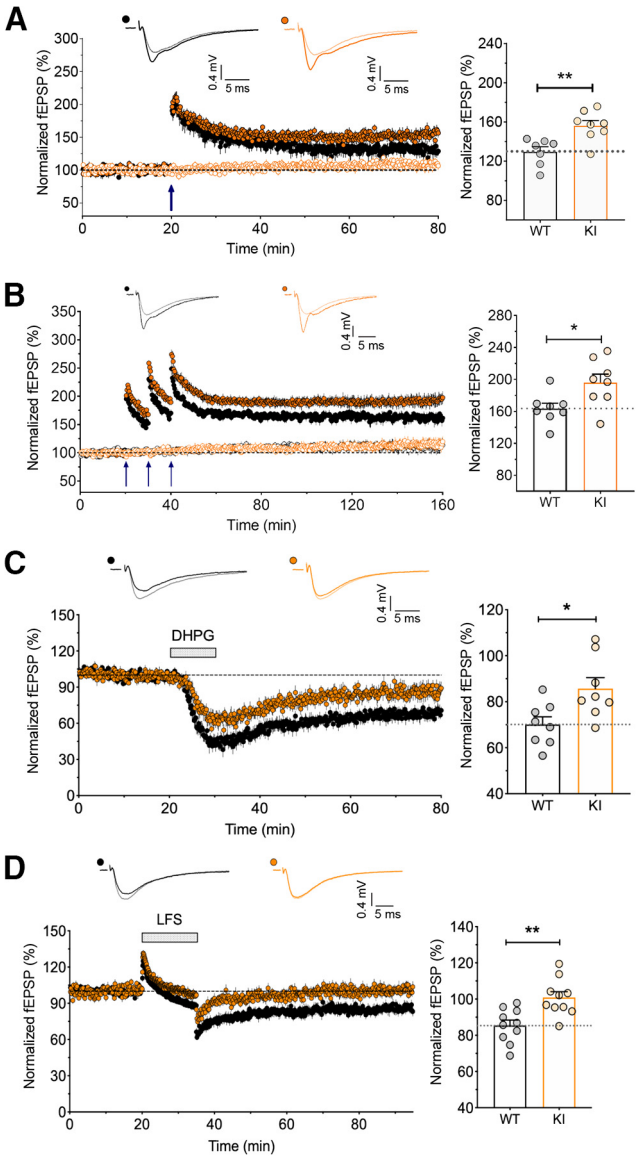

Figure 2. Enhanced LTP and reduced LTD in GluA1 K868R knock-in mice. ***A***, Input-specific LTP induced by a single episode of TBS (5 bursts at 5 Hz, with each burst composed of 5 pulses at 100 Hz). Quantification for the levels of LTP in WT ($n = 7$ from 7 mice) and KI hippocampal slices ($n = 8/8$). $^{**}p = 0.004$ (unpaired t test). ***B***, Input-specific LTP induced by three episodes of TBS with a 10 min interepisode interval and monitored for 2 h following LTP induction. Right, Significantly larger LTP in the GluA1 KI mice ($n = 8/8$) compared with those WT littermates ($n = 8/7$). Data are mean ± SEM. $^{*}p = 0.0188$ (unpaired t test). ***C***, LTD was induced by the bath application of DHPG (100 μM) + D-AP5 (50 μM). Right, Quantification of the levels of LTD. Data are mean ± SEM (WT, $n = 8/8$; KI, $n = 8/8$). $^{*}p = 0.017$ (unpaired t test). ***D***, LTD was induced by LFS (1 Hz for 15 min). Data are mean ± SEM (WT, $n = 10/10$; KI, $n = 10/10$). $^{**}p = 0.002$ (unpaired t test). Filled black circles represent WT test pathway; open black circles represent WT control pathway; filled orange circles represent KI test pathway; open orange circles represent KI control pathway.

that GluA1 ubiquitination on Lys-868 involved the covalent attachment of the K63-linked polyubiquitin chains (Fig. 1*F*,*G*). In contrast, this mutation did not affect AMPA-induced ubiquitination of the GluA2 subunit of AMPARs (Fig. 1*H*,*I*). The GluA1 ubiquitination mutant mice showed no overt behavioral phenotype and bred normally. At 3 months of age, these knock-in mice did not display any gross brain abnormalities or significant differences in the cytoarchitecture of Nissl-stained brain sections (Fig. 1*J*). These knock-in mice also had normal body weight compared with their WT littermates (Fig. 1*K*). Together, these results

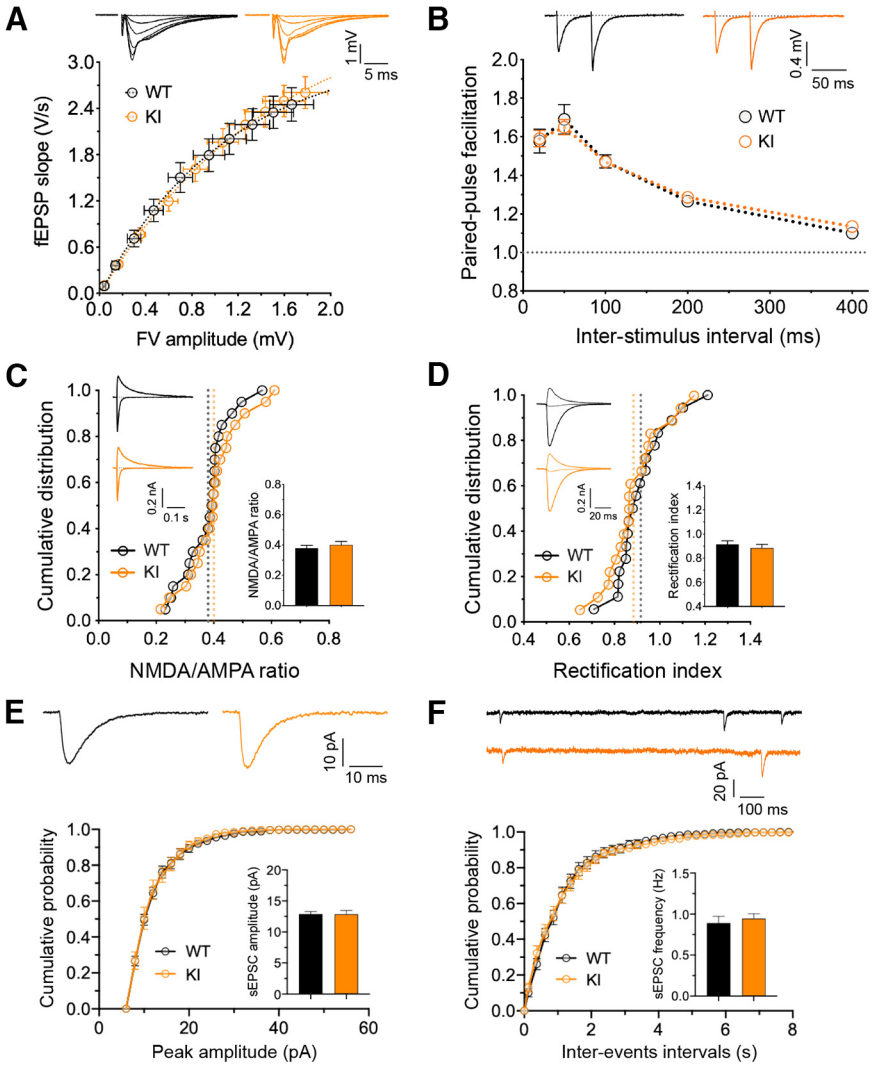

Figure 3. Intact basal synaptic properties in GluA1 K868R mutant mice. ***A***, Input–output relationships of evoked fEPSP responses at CA1 synapses for WT (black circles; $n = 10$ from 10 mice) and GluA1 K868R KI (orange circles; $n = 10/10$) littermates (male, 2-3 months old). Insets, Representative traces (averages of four successive sweeps). The stimulus intensity is represented by fiber volley (FV) amplitude. ***B***, Paired-pulse facilitation estimated at interstimulus intervals of 20, 50, 100, 200, and 400 ms (WT, $n = 10/10$; KI, $n = 10/10$). ***C***, NMDA/AMPA ratio measurements in the presence of picrotoxin (50 μM) + (+)-bicuculline (10 μM) for $GABA_A$ receptor inhibition by varying holding potentials from −70 to 40 mV. Data are mean ± SEM (WT, $n = 20/13$; KI, $n = 20/13$). $p = 0.46$ (unpaired t test). ***D***, AMPAR rectification measured in the presence of D-AP5 (50 μM) + L-689560 (5 μM) for NMDAR inhibition in addition to the $GABA_A$ receptor blockers. AMPAR currents were measured at −70, 0, and 40 mV. Data are mean ± SEM (WT, $n = 18/13$; KI, $n = 18/13$). $p = 0.44$ (unpaired t test). ***E***, ***F***, Amplitude (***E***) and frequency (***F***) of mEPSC recordings in the presence of TTX (0.5 μM). Data are mean ± SEM (WT, $n = 17/4$; KI, $n = 13/5$). $p = 0.945$ (***E***) and $p = 0.613$ (***F***) (unpaired t test).

suggest that the lack of GluA1 ubiquitination has no effect on gross brain anatomy.

To determine whether the lack of a major GluA1 ubiquitination site changes the distribution of AMPARs at postsynapses, we performed biochemical subcellular fractionation on forebrain tissues of GluA1 knock-in and WT mice. Enrichment of the postsynaptic marker PSD-95 and the absence of the presynaptic marker synaptophysin in the PSD fraction demonstrated the purity of this fraction in our preparation. We observed similar levels of GluA1, GluA2, PSD-95, and synaptophysin proteins in the total homogenate, crude synaptosomal (P2) and PSD fractions (Fig. 1*L*,*M*). These data demonstrate that the ubiquitination of GluA1 is not critical for maintaining the steady-state level of synaptic AMPARs under basal conditions *in vivo*, consistent with our previous findings in primary neuronal cultures (Widagdo et al., 2015).

LTP is enhanced and LTD is reduced in GluA1 K868R knock-in mice

We next examined the role of GluA1 ubiquitination on Lys-868 on the expression of LTP and LTD in adult male mice. We first used a single episode of TBS (5 bursts at 5 Hz, with each burst composed of 5 pulses at 100 Hz) to induce LTP, revealing a significant enhancement of input-specific LTP in hippocampal slices from GluA1 knock-in mice compared with their WT littermates (Fig. 2*A*). Moreover, LTP induced by three episodes of TBS with a 10 min interepisode interval, which is dependent on the activity of protein kinase A and new protein synthesis (Park et al., 2014), was also greatly enhanced in the GluA1 knock-in slices (Fig. 2*B*). In contrast, both NMDAR- and mGluR-dependent LTD induced by LFS and bath application of DHPG, respectively, were impaired in GluA1 knock-in slices (Fig. 2*C*,*D*).

To confirm that the enhanced LTP and deficits in LTD in the adult GluA1 ubiquitination-deficient mice were not because of nonspecific effects on synaptic transmission, we investigated the basal synaptic properties of hippocampal slices prepared from these mice. Extracellular field potential recordings with varying stimulus intensity generated identical input–output curves from homozygous knock-in mice and their WT littermates (Fig. 3*A*). We also found no change in paired-pulse facilitation across different interstimulus intervals (Fig. 3*B*). These data suggest that GluA1 ubiquitination does not affect the number of Schaffer collateral-CA1 synaptic connections or short-term presynaptic plasticity. We then performed whole-cell recordings and measured the ratio of NMDAR to AMPAR-mediated synaptic currents, revealing no statistical differences between the GluA1 knock-in and WT neurons (Fig. 3*C*). In addition, the rectification index of AMPARs was also unchanged in GluA1 knock-in neurons (Fig. 3*D*), suggesting that GluA1 ubiquitination does not affect the recruitment of Ca^{2+}-permeable GluA1 homomers to the synapse under basal conditions. Furthermore, we observed no significant differences in either the average amplitude or frequency of mEPSCs between GluA1 knock-in and WT neurons (Fig. 3*E*,*F*). Collectively, these data suggest that alterations in bidirectional synaptic plasticity are not because of abnormalities in basal synaptic transmission or NMDAR-mediated responses but are likely to be caused by the absence of ubiquitination-dependent regulation of GluA1 function during LTP and LTD.

GluA1 K868R knock-in mice exhibit cognitive deficits

Given the profound alterations in LTP and LTD in the hippocampal CA1 region, we next sought to determine whether the mutation of GluA1 on Lys-868 alters any cognitive functions in

the brain using a battery of behavioral tests (Fig. 4*A*). We first subjected these mice to the elevated plus maze and open field tests to assess their general anxiety-related behavior and locomotion. No obvious differences in anxiety levels (Fig. 4*B–D*) or locomotor activity (Fig. 4*E–H*) were observed in GluA1 knock-in mice compared with their WT littermates. We then examined hippocampal-dependent cognitive performance in the GluA1 knock-in mice. First, we used the Y-maze novelty preference test to measure short-term spatial memory, in which mice are allowed to explore the previously unvisited novel (blocked) and previously visited arms (Kraeuter et al., 2019) (Fig. 5*A*). When tested 90 min after the training sessions, both WT and GluA1 knock-in mice entered the starting and novel arms with similar frequencies (Fig. 5*B*). However, the WT, but not the homozygous mutant mice spent significantly more time in the novel arm (Fig. 5*C*), suggesting that the GluA1 ubiquitin-deficient mice have impaired short-term memory.

To further examine the cognitive performance of GluA1 knock-in mice, we conducted an active place avoidance test, a well-established hippocampal-dependent spatial memory task (Willis et al., 2017). This experiment was designed to include a reversal-learning task to test the cognitive flexibility of the mice (Fig. 5*D*). Both WT and GluA1 knock-in mice exhibited robust learning over 5 d, as evidenced by a significant decrease in the number of entries into the shock zone (Fig. 5*E*). However, when the shock zone was moved to the opposite quadrant during reversal learning (days 7-10), GluA1 knock-in mice learned to avoid the shock zone but committed significantly more errors than WT mice (Fig. 5*F*). This suggests a specific deficit in cognitive flexibility in the GluA1 mutant mice. No significant difference in total distance traveled during the test period was noted between the genotypes, indicating that locomotion was not affected (Fig. 5*G*).

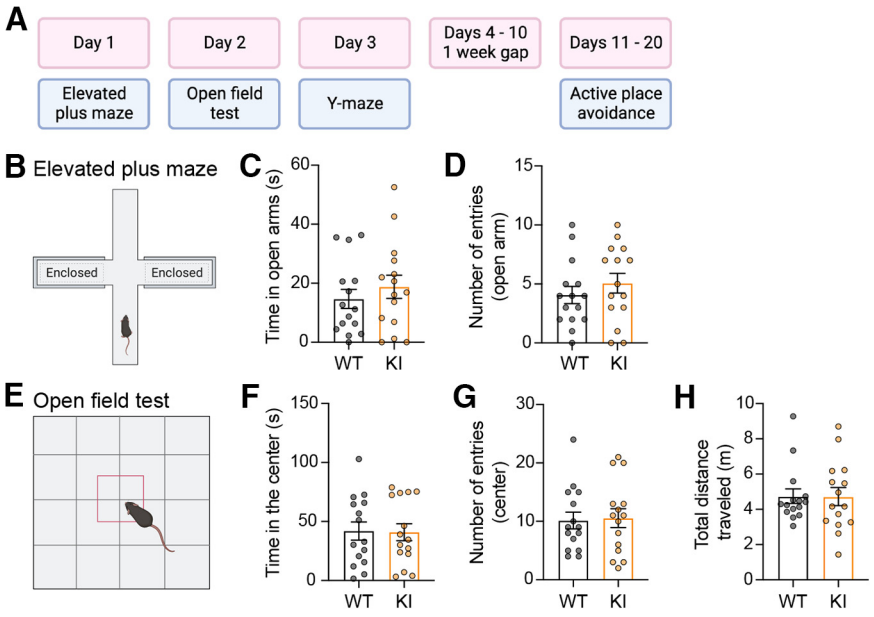

Figure 4. GluA1 K868R knock-in mice display normal locomotor activity and anxiety-like behavior. ***A***, Schematic diagram of the experimental timeline. ***B-D***, Measurement of anxiety-like behavior using the elevated plus maze (***B***) revealed no differences in the time spent in (***C***) or the number of entries to (***D***) the open arms between genotypes. Data are mean ± SEM (WT, $n = 15$; KI, $n = 15$). $p = 0.486$ (***C***) and $p = 0.380$ (***D***) (Mann–Whitney tests). ***E-H***, Measurement of locomotor activity and anxiety-like behavior using the open field test (***E***) revealed no differences in the time spent in (***F***) or the number of entries into (***G***) the central zone, or the total distance traveled (***H***) between genotypes. Data are mean ± SEM (WT, $n = 15$; KI, $n = 15$). $p = 0.806$ (***F***), $p = 0.91$ (***G***), and $p = 0.87$ (***H***) (Mann–Whitney tests).

Discussion

Upon ligand binding, the Lys-868 residue in the C-terminal tail of GluA1 is covalently modified by K63-linked polyubiquitination, which in turn regulates the post-endocytic sorting of AMPARs toward late endosomes for degradation (Schwarz et al., 2010; Widagdo et al., 2015, 2017). However, the physiological importance of GluA1 ubiquitination in neurotransmission, synaptic plasticity, learning, and memory remains unknown. In this study, we generated and characterized GluA1 K868R ubiquitin-deficient knock-in mice. Our analysis revealed that these mice have normal gross brain cytoarchitecture, intact basal synaptic transmission and breed normally. However, the GluA1 mutant mice exhibit enhanced LTP and impaired LTD. Although these mice display normal hippocampal-dependent spatial learning, they have impairments in short-term memory and cognitive flexibility. Our findings therefore demonstrate the critical roles of ubiquitin-mediated post-endocytic sorting and degradation of AMPARs in synaptic plasticity and cognition.

The role of GluA1 ubiquitination in regulating the surface expression and turnover of AMPARs under basal conditions remains controversial (Widagdo et al., 2017). Our current findings are largely in line with our previous data demonstrating that mutation of the GluA1 ubiquitination site does not alter the basal turnover and surface expression of AMPARs in primary neuronal cultures (Widagdo et al., 2015), but are in contrast to the results reported in other studies (Schwarz et al., 2010; Lin et al., 2011). First, we did not observe any changes in the protein expression of either GluA1 or GluA2 in the crude synaptosomal and PSD fractions in the forebrain of GluA1 knock-in mice. Second, we found that basal synaptic transmission in the CA3-CA1 synapses in the hippocampus of these mice remains intact, with no significant differences in spontaneous or evoked AMPAR-mediated synaptic currents. We also observed no significant changes in the rectification index of AMPARs, indicating that GluA1 ubiquitination does not regulate the subunit composition of AMPARs at the synapse under basal conditions. This is not surprising given that ubiquitination of GluA1 occurs at extremely low levels under basal conditions and is only induced on ligand binding to the AMPARs.

AMPAR recycling is essential for the maintenance of both LTP and LTD (Park et al., 2004; Brown et al., 2007; Petrini et al., 2009; Fernandez-Monreal et al., 2012; Parkinson and Hanley, 2018). Fundamentally, endosomal recycling of AMPAR-containing vesicles provides a constant supply of AMPARs to the plasma membrane to maintain LTP, while the sorting of AMPARs into late endosomes for lysosomal degradation leads to a reduction in synaptic strength that is associated with LTD. The fact that GluA1 knock-in mice have enhanced LTP and deficits in LTD is entirely consistent with the effect of K868R mutation that redirects the fate of AMPAR-containing vesicles from the degradative to the recycling pathway in neurons, thereby stabilizing the number of AMPARs on the plasma membrane following

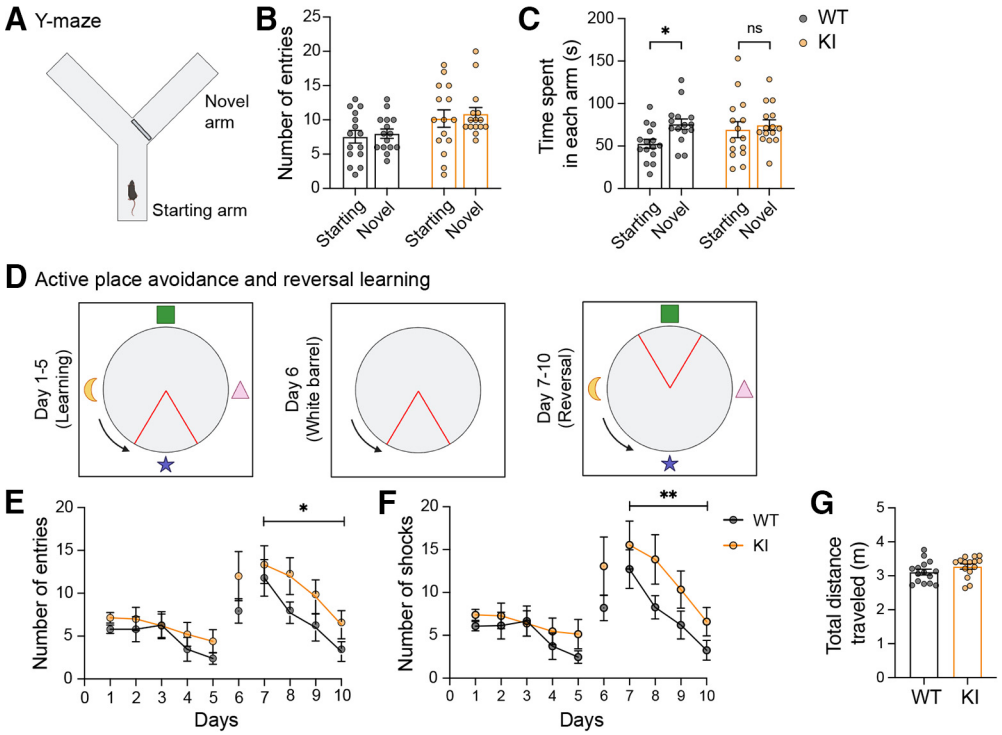

Figure 5. GluA1 K868R mutant mice exhibit cognitive deficits. ***A-C***, Measurement of short-term spatial working memory using the Y-maze with an initially blocked arm (***A***). Both WT and GluA1 KI littermates exhibited similar number of entries into the starting and the novel arms when opened (***B***). However, GluA1 WT, but not the KI mice, spent significantly more time in the novel arm (***C***). $^{*}p = 0.044$ (two-way ANOVA with Sidak's multiple comparison test). ***D***, Schematic representation of the experimental design for the active place avoidance and reversal learning tasks. The arena contained visual cues on each side of the wall. Blue arrows indicate arena rotation. Red triangles represent shock zone location. ***E***, ***F***, GluA1 KI mice displayed normal learning during the first 5 d but had significantly more entries into the shock zone (***E***) and shocks received (***F***) during reversal learning. $F_{(1,112)} = 6.033$, $^{*}p = 0.016$ (***E***) and $F_{(1,112)} = 7.278$, $^{**}p = 0.0081$ (***F***) (two-way ANOVA test). ***G***, There was no difference in the total distance traveled during the task (Mann–Whitney test, $p = 0.16$). Data are mean ± SEM ($n = 15$ mice per group).

neuronal activity (Schwarz et al., 2010; Widagdo et al., 2015). Our data also imply that a fraction of internalized GluA1-containing AMPARs is ubiquitinated and destined for lysosomal degradation, presumably to prevent excessive AMPARs from being inserted into the plasma membrane during LTP. Our findings also establish the requirement of GluA1 ubiquitination in mediating both NMDAR- and mGluR-dependent LTD. Although direct stimulation of primary neurons with NMDA and DHPG is not sufficient to induce GluA1 ubiquitination to a level detectable by Western blotting, bicuculline-induced ubiquitination of GluA1 does involve NMDAR- and mGluR-dependent signaling (Widagdo et al., 2015).

GluA1 ubiquitination is not only important for LTP and LTD but also contributes to spatial and short-term memory. This is consistent with the synaptic plasticity and memory hypothesis, which posits that activity-dependent and bidirectional changes in the weights of relevant synapses mediate the formation, reactivation, and update of memory of prior experiences (Takeuchi et al., 2014). In the novelty preference task, GluA1 K868R knock-in mice did not show any preference to explore the novel arm during the test session. This phenotype can be explained by the enhanced LTP phenotype associated with these mice. Consistent with the observation that the mutant mice display augmentation of NMDAR-dependent LTP (Migaud et al., 1998; Garcia-Alvarez et al., 2015), our data suggest the potential role of "saturated" LTP that prevents the encoding or updating of new information in the short term (Barnes et al., 1994; Bannerman et al., 2014). Paradoxically, a similar impairment in short-term spatial memory has also been reported in GluA1 KO mice, which exhibit deficits in LTP (Sanderson et al., 2009; Bannerman et al., 2014). These findings underscore the physiological importance of the ability of synapses to undergo bidirectional plasticity for efficient information processing, learning, and memory.

Using the active place avoidance behavioral task, we found that the GluA1 knock-in mice perform as well as their WT littermates, indicating that hippocampal-dependent spatial learning is intact in these ubiquitin-deficient mutant mice. These findings are consistent with the normal spatial learning reported in GluA1 KO and S831/845A phospho-deficient mutant mice (Zamanillo et al., 1999; Reisel et al., 2002; Lee et al., 2003). However, we observed that reversal learning was impaired in the GluA1 ubiquitin-deficient mutant, in association with deficits in both NMDAR- and mGluR-mediated LTD. This is interesting considering that deficits in behavioral flexibility are often accompanied by defective GluA1 endocytosis and deficits in LTD (Nicholls et al., 2008; Xu et al., 2009; Collingridge et al., 2010; Kim et al., 2011; Eales et al., 2014; Mills et al., 2014; Awasthi et al., 2019). However, it is worth noting that enhanced mGluR-dependent LTD because of excessive internalization of surface AMPARs can also result in an impairment in reversal learning and cognitive flexibility (Wall et al., 2018). Together, our results indicate that the correct targeting and endosomal recycling of AMPARs to the postsynaptic membrane through the ubiquitination of GluA1 are necessary for bidirectional synaptic plasticity and the expression of rapidly learned spatial memory, memory updating, and cognitive flexibility.

Several lines of evidence have demonstrated the direct involvement of AMPAR ubiquitination as a critical pathway in mediating Aβ-induced synaptic depression in neurons. First, the expression of Nedd4-1 is upregulated in the human Alzheimer's brain, which

correlates with an increase in AMPAR ubiquitination and a decrease in total AMPAR protein levels (Kwak et al., 2012; Zhang et al., 2018). Second, knocking down the expression of Nedd4-1 abolishes the Aβ-induced reduction in the levels of surface AMPARs, AMPAR-mediated currents, and dendritic spine loss (Rodrigues et al., 2016; Zhang et al., 2018). Third, acute exposure of cultured neurons to soluble Aβ oligomers induces AMPAR ubiquitination concomitant with the removal of these receptors from the plasma membrane (Guntupalli et al., 2017). Importantly, the expression of GluA1-K868R ubiquitin-deficient mutants inhibits the adverse effects of Aβ on the surface expression of AMPARs in neurons. Therefore, the GluA1 K868R knock-in mice we have generated will be useful for determining whether inhibiting the ubiquitination of AMPARs is a viable strategy to prevent the effects of Aβ on cognitive functions in mouse models of Alzheimer's disease.

References

Anderson WW, Collingridge GL (2007) Capabilities of the WinLTP data acquisition program extending beyond basic LTP experimental functions. J Neurosci Methods 162:346–356.

Anggono V, Huganir RL (2012) Regulation of AMPA receptor trafficking and synaptic plasticity. Curr Opin Neurobiol 22:461–469.

Awasthi A, Ramachandran B, Ahmed S, Benito E, Shinoda Y, Nitzan N, Heukamp A, Rannio S, Martens H, Barth J, Burk K, Wang YT, Fischer A, Dean C (2019) Synaptotagmin-3 drives AMPA receptor endocytosis, depression of synapse strength, and forgetting. Science 363:eaav1483.

Bannerman DM, Sprengel R, Sanderson DJ, McHugh SB, Rawlins JN, Monyer H, Seeburg PH (2014) Hippocampal synaptic plasticity, spatial memory and anxiety. Nat Rev Neurosci 15:181–192.

Barnes CA, Jung MW, McNaughton BL, Korol DL, Andreasson K, Worley PF (1994) LTP saturation and spatial learning disruption: effects of task variables and saturation levels. J Neurosci 14:5793–5806.

Brown TC, Correia SS, Petrok CN, Esteban JA (2007) Functional compartmentalization of endosomal trafficking for the synaptic delivery of AMPA receptors during long-term potentiation. J Neurosci 27:13311–13315.

Collingridge GL, Peineau S, Howland JG, Wang YT (2010) Long-term depression in the CNS. Nat Rev Neurosci 11:459–473.

Diering GH, Huganir RL (2018) The AMPA receptor code of synaptic plasticity. Neuron 100:314–329.

Eales KL, Palygin O, O'Loughlin T, Rasooli-Nejad S, Gaestel M, Muller J, Collins DR, Pankratov Y, Correa SA (2014) The MK2/3 cascade regulates AMPAR trafficking and cognitive flexibility. Nat Commun 5:4701.

Fernandez-Monreal M, Brown TC, Royo M, Esteban JA (2012) The balance between receptor recycling and trafficking toward lysosomes determines synaptic strength during long-term depression. J Neurosci 32:13200–13205.

Garcia-Alvarez G, Shetty MS, Lu B, Yap KA, Oh-Hora M, Sajikumar S, Bichler Z, Fivaz M (2015) Impaired spatial memory and enhanced long-term potentiation in mice with forebrain-specific ablation of the Stim genes. Front Behav Neurosci 9:180.

Goo MS, Scudder SL, Patrick GN (2015) Ubiquitin-dependent trafficking and turnover of ionotropic glutamate receptors. Front Mol Neurosci 8:60.

Guntupalli S, Jang SE, Zhu T, Huganir RL, Widagdo J, Anggono V (2017) GluA1 subunit ubiquitination mediates amyloid-β-induced loss of surface α-amino-3-hydroxy-5-methyl-4-isoxazolepropionic acid (AMPA) receptors. J Biol Chem 292:8186–8194.

Hayashi T (2021) Post-translational palmitoylation of ionotropic glutamate receptors in excitatory synaptic functions. Br J Pharmacol 178:784–797.

Hu H, Real E, Takamiya K, Kang MG, Ledoux J, Huganir RL, Malinow R (2007) Emotion enhances learning via norepinephrine regulation of AMPA-receptor trafficking. Cell 131:160–173.

Huganir RL, Nicoll RA (2013) AMPARs and synaptic plasticity: the last 25 years. Neuron 80:704–717.

Kim JI, et al. (2011) PI3Kgamma is required for NMDA receptor-dependent long-term depression and behavioral flexibility. Nat Neurosci 14:1447–1454.

Kraeuter AK, Guest PC, Sarnyai Z (2019) The Y-maze for assessment of spatial working and reference memory in mice. Methods Mol Biol 1916:105–111.

Kristensen AS, Jenkins MA, Banke TG, Schousboe A, Makino Y, Johnson RC, Huganir R, Traynelis SF (2011) Mechanism of Ca^{2+}/calmodulin-dependent kinase II regulation of AMPA receptor gating. Nat Neurosci 14:727–735.

Kwak YD, Wang B, Li JJ, Wang R, Deng Q, Diao S, Chen Y, Xu R, Masliah E, Xu H, Sung JJ, Liao FF (2012) Upregulation of the E3 ligase NEDD4-1 by oxidative stress degrades IGF-1 receptor protein in neurodegeneration. J Neurosci 32:10971–10981.

Lee HK, Barbarosie M, Kameyama K, Bear MF, Huganir RL (2000) Regulation of distinct AMPA receptor phosphorylation sites during bidirectional synaptic plasticity. Nature 405:955–959.

Lee HK, Takamiya K, Han JS, Man H, Kim CH, Rumbaugh G, Yu S, Ding L, He C, Petralia RS, Wenthold RJ, Gallagher M, Huganir RL (2003) Phosphorylation of the AMPA receptor GluR1 subunit is required for synaptic plasticity and retention of spatial memory. Cell 112:631–643.

Lin A, Hou Q, Jarzylo L, Amato S, Gilbert J, Shang F, Man HY (2011) Nedd4-mediated AMPA receptor ubiquitination regulates receptor turnover and trafficking. J Neurochem 119:27–39.

Lu W, Roche KW (2012) Posttranslational regulation of AMPA receptor trafficking and function. Curr Opin Neurobiol 22:470–479.

Lu W, Shi Y, Jackson AC, Bjorgan K, During MJ, Sprengel R, Seeburg PH, Nicoll RA (2009) Subunit composition of synaptic AMPA receptors revealed by a single-cell genetic approach. Neuron 62:254–268.

Lussier MP, Sanz-Clemente A, Roche KW (2015) Dynamic regulation of N-methyl-d-aspartate (NMDA) and α-amino-3-hydroxy-5-methyl-4-isoxazolepropionic acid (AMPA) receptors by posttranslational modifications. J Biol Chem 290:28596–28603.

Ma P, Wan LP, Li Y, He CH, Song NN, Zhao S, Wang H, Ding YQ, Mao B, Sheng N (2022) RNF220 is an E3 ubiquitin ligase for AMPA receptors to regulate synaptic transmission. Sci Adv 8:eabq4736.

Mabb AM (2021) Historical perspective and progress on protein ubiquitination at glutamatergic synapses. Neuropharmacology 196:108690.

Makino Y, Johnson RC, Yu Y, Takamiya K, Huganir RL (2011) Enhanced synaptic plasticity in mice with phosphomimetic mutation of the GluA1 AMPA receptor. Proc Natl Acad Sci USA 108:8450–8455.

Man HY, Sekine-Aizawa Y, Huganir RL (2007) Regulation of α-amino-3-hydroxy-5-methyl-4-isoxazolepropionic acid receptor trafficking through PKA phosphorylation of the Glu receptor 1 subunit. Proc Natl Acad Sci USA 104:3579–3584.

Migaud M, Charlesworth P, Dempster M, Webster LC, Watabe AM, Makhinson M, He Y, Ramsay MF, Morris RG, Morrison JH, O'Dell TJ, Grant SG (1998) Enhanced long-term potentiation and impaired learning in mice with mutant postsynaptic density-95 protein. Nature 396:433–439.

Mills F, Bartlett TE, Dissing-Olesen L, Wisniewska MB, Kuznicki J, Macvicar BA, Wang YT, Bamji SX (2014) Cognitive flexibility and long-term depression (LTD) are impaired following beta-catenin stabilization in vivo. Proc Natl Acad Sci USA 111:8631–8636.

Nicholls RE, Alarcon JM, Malleret G, Carroll RC, Grody M, Vronskaya S, Kandel ER (2008) Transgenic mice lacking NMDAR-dependent LTD exhibit deficits in behavioral flexibility. Neuron 58:104–117.

Park M, Penick EC, Edwards JG, Kauer JA, Ehlers MD (2004) Recycling endosomes supply AMPA receptors for LTP. Science 305:1972–1975.

Park P, Volianskis A, Sanderson TM, Bortolotto ZA, Jane DE, Zhuo M, Kaang BK, Collingridge GL (2014) NMDA receptor-dependent long-term potentiation comprises a family of temporally overlapping forms of synaptic plasticity that are induced by different patterns of stimulation. Philos Trans R Soc Lond B Biol Sci 369:20130131.

Park P, Sanderson TM, Amici M, Choi SL, Bortolotto ZA, Zhuo M, Kaang BK, Collingridge GL (2016) Calcium-permeable AMPA receptors mediate the induction of the protein kinase A-dependent component of long-term potentiation in the hippocampus. J Neurosci 36:622–631.

Parkinson GT, Hanley JG (2018) Mechanisms of AMPA receptor endosomal sorting. Front Mol Neurosci 11:440.

Petrini EM, Lu J, Cognet L, Lounis B, Ehlers MD, Choquet D (2009) Endocytic trafficking and recycling maintain a pool of mobile surface AMPA receptors required for synaptic potentiation. Neuron 63:92–105.

Reisel D, Bannerman DM, Schmitt WB, Deacon RM, Flint J, Borchardt T, Seeburg PH, Rawlins JN (2002) Spatial memory dissociations in mice lacking GluR1. Nat Neurosci 5:868–873.

Rodrigues EM, Scudder SL, Goo MS, Patrick GN (2016) Aβ-induced synaptic alterations require the E3 ubiquitin ligase Nedd4-1. J Neurosci 36:1590–1595.

Sanderson DJ, Gray A, Simon A, Taylor AM, Deacon RM, Seeburg PH, Sprengel R, Good MA, Rawlins JN, Bannerman DM (2007) Deletion of glutamate receptor-A (GluR-A) AMPA receptor subunits impairs one-trial spatial memory. Behav Neurosci 121:559–569.

Sanderson DJ, Good MA, Skelton K, Sprengel R, Seeburg PH, Rawlins JN, Bannerman DM (2009) Enhanced long-term and impaired short-term spatial memory in GluA1 AMPA receptor subunit knockout mice: evidence for a dual-process memory model. Learn Mem 16:379–386.

Sanderson DJ, McHugh SB, Good MA, Sprengel R, Seeburg PH, Rawlins JN, Bannerman DM (2010) Spatial working memory deficits in GluA1 AMPA receptor subunit knockout mice reflect impaired short-term habituation: evidence for Wagner's dual-process memory model. Neuropsychologia 48:2303–2315.

Schwarz LA, Hall BJ, Patrick GN (2010) Activity-dependent ubiquitination of GluA1 mediates a distinct AMPA receptor endocytosis and sorting pathway. J Neurosci 30:16718–16729.

Schwenk F, Baron U, Rajewsky K (1995) A cre-transgenic mouse strain for the ubiquitous deletion of loxP-flanked gene segments including deletion in germ cells. Nucleic Acids Res 23:5080–5081.

Takeuchi T, Duszkiewicz AJ, Morris RG (2014) The synaptic plasticity and memory hypothesis: encoding, storage and persistence. Philos Trans R Soc Lond B Biol Sci 369:20130288.

Wall MJ, Collins DR, Chery SL, Allen ZD, Pastuzyn ED, George AJ, Nikolova VD, Moy SS, Philpot BD, Shepherd JD, Muller J, Ehlers MD, Mabb AM, Correa SA (2018) The temporal dynamics of Arc expression regulate cognitive flexibility. Neuron 98:1124–1132.e7.

Widagdo J, Chai YJ, Ridder MC, Chau YQ, Johnson RC, Sah P, Huganir RL, Anggono V (2015) Activity-dependent ubiquitination of GluA1 and GluA2 regulates AMPA receptor intracellular sorting and degradation. Cell Rep 10:783–795.

Widagdo J, Guntupalli S, Jang SE, Anggono V (2017) Regulation of AMPA receptor trafficking by protein ubiquitination. Front Mol Neurosci 10:347.

Widagdo J, Kerk JW, Guntupalli S, Huganir RL, Anggono V (2020) Subunit-specific augmentation of AMPA receptor ubiquitination by phorbol ester. Cell Mol Neurobiol 40:1213–1222.

Willis EF, Bartlett PF, Vukovic J (2017) Protocol for short- and longer-term spatial learning and memory in mice. Front Behav Neurosci 11:197.

Xu J, Zhu Y, Contractor A, Heinemann SF (2009) mGluR5 has a critical role in inhibitory learning. J Neurosci 29:3676–3684.

Zamanillo D, Sprengel R, Hvalby O, Jensen V, Burnashev N, Rozov A, Kaiser KM, Koster HJ, Borchardt T, Worley P, Lubke J, Frotscher M, Kelly PH, Sommer B, Andersen P, Seeburg PH, Sakmann B (1999) Importance of AMPA receptors for hippocampal synaptic plasticity but not for spatial learning. Science 284:1805–1811.

Zhang Y, Guo O, Huo Y, Wang G, Man HY (2018) Amyloid-β induces AMPA receptor ubiquitination and degradation in primary neurons and human brains of Alzheimer's disease. J Alzheimers Dis 62:1789–1801.

Zhu J, Lee KY, Jewett KA, Man HY, Chung HJ, Tsai NP (2017) Epilepsy-associated gene Nedd4-2 mediates neuronal activity and seizure susceptibility through AMPA receptors. PLoS Genet 13:e1006634.